C-Terminal Region Amino Acid Substitutions Contribute to Catalytic Differences between Murine Class Alpha Glutathione Transferases mGSTA1-1 and mGSTA2-2 toward *anti*-Diol Epoxide Isomers of Benzo[*c*]phenanthrene†

Ajai Pal,‡ Yijun Gu,‡ Su-Shu Pan,‡ Xinhua Ji,§ and Shivendra V. Singh*,‡

Department of Pharmacology and University of Pittsburgh Cancer Institute, University of Pittsburgh School of Medicine, Pittsburgh, Pennsylvania 15261, and Macromolecular Crystallography Laboratory, National Cancer Institute, Frederick, Maryland 21702

Received February 21, 2001; Revised Manuscript Received April 24, 2001

ABSTRACT: The molecular basis for catalytic differences between structurally closely related murine class alpha glutathione (GSH) transferases mGSTA1-1 and mGSTA2-2 in the GSH conjugation of *anti*-diol epoxide isomers of benzo[*c*]phenanthrene (*anti*-B[*c*]PDE) was investigated. GSH conjugation of both (−)- and (+)-enantiomers of *anti*-B[*c*]PDE was observed in the presence of mGSTA1-1 (60 and 40% GSH conjugation, respectively), whereas mGSTA2-2 exhibited a preference for the (−)-*anti*-isomer (>97%). In addition, the specific activity of mGSTA2-2 toward the (−)-*anti*-B[*c*]PDE isomer was relatively higher than that of mGSTA1-1. The amino acid sequences of mGSTA1-1 and mGSTA2-2 differ at 10 positions that are distributed in three sections. Section I contains amino acid residues in positions 65 and 95; section II contains residues in positions 157, 162, and 169, and section III contains residues in positions 207, 213, 218, 221, and 222. Enzyme activity measurements with chimeras of mGSTA1-1 and mGSTA2-2 revealed that amino acid substitutions in section III account for their differential enantioselectivity and catalytic activity toward *anti*-B[*c*]PDE. Site-directed mutagenesis of amino acid residues in section III of mGSTA2-2 with corresponding residues of mGSTA1-1 followed by activity measurements of the wild type and mutated enzymes indicates that leucine 207 and phenylalanine 221 may be critical for the high catalytic activity of mGSTA2-2 toward (−)-*anti*-B[*c*]PDE. Molecular modeling studies demonstrated that the active site of mGSTA1-1 accommodates both enantiomers of *anti*-B[*c*]PDE, whereas the (−)-*anti*-isomer interacts more favorably with active site residues in mGSTA2-2. The results of this study clearly indicate that amino acid substitutions in the C-terminal region contribute to catalytic differences between mGSTA1-1 and mGSTA2-2 with respect to *anti*-B[*c*]PDE.

Polycyclic aromatic hydrocarbons (PAHs),[1] such as benzo[*c*]phenanthrene (B[*c*]P), are widespread environmental pollutants that are tumorigenic in laboratory animals and believed to be risk factors in human chemical carcinogenesis (*1*−*3*). Tumorigenic activity of many PAHs, including B[*c*]P, is attributed to their respective diol epoxides, which are formed through catalytic mediation of cytochrome P450-dependent monooxygenases and epoxide hydrolase (*3*−*5*). For example, 3,4-dihydroxy-1,2-epoxy-1,2,3,4-tetrahydrobenzo[*c*]phenanthrene (B[*c*]PDE) is the activated diol epoxide metabolite of B[*c*]P (*3*). PAH diol epoxides implicated in chemical carcinogenesis, including B[*c*]PDE, can be resolved into a pair of optical enantiomers [(+)- and (−)-enantiomers] of two diastereomers (*anti*- and *syn*-isomers). Systematic examinations of optically pure isomers of B[*c*]PDE have clearly shown that the (−)-*anti*-stereoisomer of B[*c*]PDE with (1*R*,2*S*)-epoxide (3*S*,4*R*)-diol absolute configuration [see Chart 1 for structures and absolute configurations of the (+)- and (−)-*anti*-isomers of B[*c*]PDE] is a more potent tumor initiator than other isomers in the newborn mouse model (*3*). Likewise, (−)-*anti*-B[*c*]PDE is significantly more active in skin-tumorigenesis bioassays than (+)-*anti*-B[*c*]PDE with the (1*S*,2*R*)-epoxide (3*R*,4*S*)-diol absolute configuration (*3*). While covalent interaction of the diol epoxides with nucleophilic sites in DNA is critical in the initiation of cancers induced by PAHs (*6*), a number of mechanisms exist that can prevent this interaction (*7*−*14*). The known mechanisms for the inactivation of PAH diol epoxides include nonenzymatic hydrolysis, epoxide hydrolase-mediated hydration, and glutathione (GSH) transferase (GST)-catalyzed conjugation with GSH (*7*−*14*). However, the GST-catalyzed GSH

† This work was supported in part by U.S. Public Health Service Grants RO1 CA76348 and RO1 CA55589 (to S.V.S.), awarded by the National Cancer Institute.

* To whom correspondence should be addressed: S-871 Scaife Hall, Box 130, University of Pittsburgh, 3550 Terrace St., Pittsburgh, PA 15261. Phone: (412) 648-3769. Fax: (412) 648-9069. E-mail: singhs@msx.upmc.edu.

‡ University of Pittsburgh.

§ National Cancer Institute.

[1] Abbreviations: B[*c*]P, benzo[*c*]phenanthrene; B[*c*]PDE, 3,4-dihydroxy-1,2-epoxy-1,2,3,4-tetrahydrobenzo[*c*]phenanthrene; (−)-*anti*-B[*c*]PDE, (1*R*,2*S*,3*S*,4*R*)-3,4-dihydroxy-1,2-epoxy-1,2,3,4-tetrahydrobenzo[*c*]phenanthrene; (+)-*anti*-B[*c*]PDE, (1*S*,2*R*,3*R*,4*S*)-3,4-dihydroxy-1,2-epoxy-1,2,3,4-tetrahydrobenzo[*c*]phenanthrene; (+)-*anti*-BPDE, (7*R*,8*S*,9*S*,10*R*)-7,8-dihydroxy-9,10-epoxy-7,8,9,10-tetrahydrobenzo[*a*]pyrene; GSH, glutathione; GST, glutathione transferase; PAHs, polycyclic aromatic hydrocarbons; SDS−PAGE, sodium dodecyl sulfate−polyacrylamide gel electrophoresis; TKE buffer, 50 mM Tris-HCl (pH 7.5) containing 2.5 mM KCl and 0.5 mM EDTA.

10.1021/bi010363r CCC: $20.00
Published on Web 05/23/2001

Chart 1

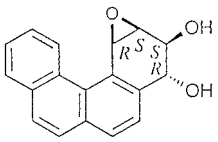

(-)-***anti***-B[c]PDE

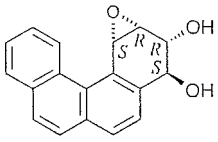

(+)-***anti***-B[c]PDE

conjugation is the most important enzymatic pathway for detoxification of PAH-diol epoxides (*10*−*14*).

GSTs are a superfamily of multifunctional isoenzymes that can catalyze the addition of GSH to a wide variety of compounds containing an electrophilic center (*15*, *16*). The cytosolic GST activity in mammalian tissues is frequently due to multiple isoenzymes that arise from dimeric combinations of either identical or structurally different subunits. Cytosolic GSTs have been grouped into various classes, namely, alpha, mu, pi, theta, and zeta, based on their structural and functional properties (*16*−*19*). GST isoenzymes of these classes differ markedly in their substrate specificities (*16*, *17*). For example, the pi class human isoenzyme hGSTP1-1 is significantly more efficient than alpha class human GSTs in catalyzing the GSH conjugation of an activated diol epoxide metabolite of benzo[*a*]pyrene (*10*).

To establish the relative contributions of GST isoenzymes in defense against carcinogenic effects of B[*c*]P, we have systematically examined specificities of different classes of murine GSTs toward B[*c*]PDE stereoisomers (*20*). The alpha class isoenzyme with an isoelectric point of 9.5 (GST 9.5) was found to be approximately 4−22-fold more active than mu and pi classes of murine GSTs in catalyzing the GSH conjugation of (−)- and (+)-enantiomers of *anti*-B[*c*]PDE (*20*). GST 9.5 is expressed at a significantly higher level in the forestomach of female A/J mice than in other tissues (*21*−*23*). This isoenzyme is a dimer of two structurally closely related alpha class subunits, A1 and A2 (*23*).

Herein, we demonstrate that the A1 and A2 subunits differ remarkably in their enantioselectivity toward *anti*-B[*c*]PDE. Furthermore, this study demonstrates that amino acid substitutions in the C-terminal region, particularly residues in positions 207 and 221, account for catalytic differences between mGSTA1-1 and mGSTA2-2 with respect to *anti*-B[*c*]PDE.

EXPERIMENTAL PROCEDURES

Chemicals. Epoxy-activated Sepharose 6B, GSH, and isopropyl β-D-thiogalactopyranoside (IPTG) were from Sigma (St. Louis, MO). (±)-*anti*-B[*c*]PDE was from Midwest Research Institute (Kansas City, MO). Restriction endonucleases and T4 DNA ligase were from New England Bio Labs, Inc. (Beverly, MA). Taq DNA polymerase was from Promega (Madison, WI). The pET-11d vector, BL21(DE3) competent cells, and PK enzyme mix were from Novagen, Inc. (Madison, WI). The Prep-A-Gene DNA purification kit was from Bio-Rad Laboratories (Hercules, CA).

Construction of Chimeras of mGSTA1-1 and mGSTA2-2. Plasmids pET-l ld/mGSTA1 and pET-11d/mGSTA2 containing the coding sequences of mGSTA1 and mGSTA2, respectively, were expanded in *Escherichia coli* DM1 and isolated by standard procedures. As shown in Table 1, the 10 amino acid differences between mGSTA1-1 and mGSTA2-2 are distributed in three sections (I−III). To replace section I of mGSTA2 with the corresponding section of mGSTA1, plasmids pET-11d/mGSTAl and pET-11d/mGSTA2 were digested with *Bgl*II, which resulted in a small fragment (about 400 bp) and a large fragment. The small fragment of pET-11d/mGSTA1 and the large fragment of pET-11d/mGSTA2 were separated on an 1% agarose gel, purified using the Prep-A-Gene DNA purification kit, and ligated using T4 DNA ligase. The resultant construct contained section I of mGSTA1-1, and sections II and III of mGSTA2-2. To replace section III of mGSTA2 with an equivalent portion of mGSTAl, plasmids pET-11d/mGSTA1 and pET-11d/mGSTA2 were digested with *Stu*I (this restriction site is located 545 bp downstream of the ATG start codon) and *Bam*HI (this site is on the pET-11d vector downstream of the mGSTA cDNA insert location). These digestions resulted in a small fragment (~160 bp) containing section III of the mGSTA cDNA insert and a small portion of the vector, and a large fragment containing the rest of the mGSTA cDNA insert and the vector. The small fragment of mGSTA1 was ligated with the *Stu*I−*Bam*HI large fragment from pET-11d/mGSTA2. Therefore, the resultant construct contained sections I and II of mGSTA2 but section III of mGSTA1. Preparation of a construct containing section II of mGSTA1 and sections I and III of mGSTA2 was achieved similarly using the restriction enzymes described above. The ligation mixtures containing chimeric constructs were transformed into BL21(DE3) competent cells, and the colonies were screened. The DNA sequence of each selected chimeric construct was confirmed by DNA sequencing. Expression of GST was detected initially by activity determinations using 1-chloro-2,4-dinitrobenzene (CDNB) as a substrate. The GST activity toward CDNB was determined by the method of Habig et al. (*24*). The protein content was determined by Bradford's method (*25*).

Table 1: Differences in Amino Acid Sequences between mGSTA1-1 and mGSTA2-2

	mGSTA1-1	mGSTA2-2
section I		
residue 65	alanine	valine
residue 95	serine	threonine
section II		
residue 157	isoleucine	valine
residue 162	valine	leucine
residue 169	phenylalanine	leucine
section III		
residue 207	methionine	leucine
residue 213	glutamine	glutamic acid
residue 218	alanine	valine
residue 221	isoleucine	phenylalanine
residue 222	glutamine	−

Site-Directed Mutagenesis. Replacement of five amino acid residues in section III of mGSTA2 with equivalents of mGSTA1 (leucine 207 to methionine, glutamic acid 213 to glutamine, valine 218 to alanine, phenyalanine 221 to isoleucine, and addition of glutamine at position 222; this last residue is present in mGSTA1-1 but absent in mGSTA2-2) was achieved by PCR-based site-directed mutagenesis as described previously (*26*). Briefly, two PCRs were performed to obtain one mutation site. Plasmid pET-11d/mGSTA2 was the template for all the mutations. Four primers, two common

Table 2: Primers Used for Site-Directed Mutagenesis[a]

mutation	primer direction	primer sequence (5′−3′)
mGSTA2/L207M	forward a2	GAAAGCCTCCCaTGGATGCAA
	reverse b1	TCTGGCTGCCAGGCTGTAGAAA
mGSTA2/E213Q	forward a2	GGATGCAAAACAAATTcAAGAAGC
	reverse b1	AAGGGAGGCTTTCTCTGGCT
mGSTA2/V218A	forward a2	GAAGCAAGGAAGGcTTTCAAG
	reverse b1	TTCAATTTGTTTTGCATCCAAGG
mGSTA2/F221I	forward a2	CAAGGAAGGTTTTCAAGaTTTAG
	reverse b1	CTTCTTCAATTTGTTTTGCATCC
mGSTA2/−222Q	forward a2	GGTTTTCAAGTTTcAGTGaGGCAA
	reverse b1	TTCCTTGCTTCTTCAATTTGTTT

[a] The common forward primer a1: CGGATAACAATTCCCCTCTAGAA. The common reverse primer b2: CAGCTTATCATCGATAAGCTT. The mutated bases in forward primer a2 are shown in lowercase letters.

primers and two site specific primers (Table 2), were needed for each mutation. The two common primers, forward a1 and reverse b2, are located in the vector containing a *Xba*I and a *Hin*dIII site, respectively. Specific forward primer a2 of each mutation site contained the designed DNA base alteration. Specific reverse primer b1 is located in mGSTA2 immediately upstream of primer a2. The first PCR used common forward primer a1 and site specific reverse primer b1 to yield a product of 0.65−0.7 kb. The second PCR used site specific forward primer a2 and common reverse primer b2 to yield a product of 0.23−0.29 kb. All PCRs were performed under the same conditions as described previously (*26*). The two PCR products of each mutation site were purified with a QIAgen PCR purification kit, and then treated with the PK enzyme mix to remove nucleotide overhangs and to phosphorylate the 5′-end. After purification, the first and second PCR products were digested with *Xba*I and *Hin*dIII, respectively, and then ligated with the large fragment of the pET-11d vector linearized by *Xba*I and *Hin*dIII. Finally, the plasmid of each mutated construct was expanded in *E. coli* BL21(DE3), and their DNA sequences were confirmed. Expression of GST was detected as described above.

GST Purification. Bacteria containing the desired construct were cultured overnight in Luria-Bertani (LB) medium supplemented with 100 μg/mL ampicillin. Cultures were diluted 1:50 with LB medium and incubated further with shaking for 2 h at 37 °C. IPTG at a final concentration of 2 mM was then added to the cultures, which were incubated with shaking for an additional 3−4 h. Bacteria were harvested by centrifugation at 800*g* for 5 min. The pellet was suspended in 50 mM Tris-HCl (pH 8.0) containing 5 mM EDTA and 50 μg/mL lysozyme, and incubated at room temperature for 15 min. The suspension was sonicated, and the lysate was centrifuged at 14000*g* for 30 min. The supernatant fraction was dialyzed overnight against 22 mM potassium phosphate buffer (pH 7.0) containing 1.4 mM 2-mercaptoethanol (affinity buffer) and subjected to affinity chromatography on a column (1.6 cm × 6.0 cm) of GSH linked to epoxy-activated Sepharose 6B. GSH affinity chromatography was performed according to the method of Simons and Vander Jagt (*27*). The GST was eluted with 5 mM GSH in 50 mM Tris-HCl (pH 9.5) containing 1.4 mM 2-mercaptoethanol. The purity of the GST preparation was ascertained by SDS−PAGE (*28*) and reverse-phase HPLC (*21*).

Determination of GST Activity toward anti-B[c]PDE. The purified GST preparation was dialyzed against 50 mM Tris-HCl (pH 7.5) containing 2.5 mM KCl and 0.5 mM EDTA (TKE buffer) prior to activity determinations. The GST activity toward *anti*-B[*c*]PDE was determined as described previously by us (*20*). Briefly, the reaction mixture in a final volume of 0.1 mL contained TKE buffer, 2 mM GSH, 320 μM (±)-*anti*-B[*c*]PDE, and GST protein (15 μg/mL). The reaction was started by adding (±)-*anti*-B[*c*]PDE. The reaction mixture was incubated for 30 s at 37 °C, and the reaction was terminated by rapid mixing with 0.1 mL of cold acetone. Subsequently, the reaction mixture was extracted twice with ethyl acetate to remove unreacted diol epoxide. The GSH conjugates of (+)- and (−)-*anti*-B[*c*]PDE in the aqueous phase were quantified by reverse-phase HPLC as described previously by us (*20*). Standards of GSH conjugates of the (−)- and (+)-*anti*-isomers of B[*c*]PDE were subjected to reverse-phase HPLC to establish their identity and retention times. A control without the GST protein was included to account for nonenzymatic conjugation of diol epoxides with GSH.

Molecular Modeling. The molecular modeling studies were carried out with program suites X-PLOR (*29*) and O (*30*) on an SGI Indigo2 Impact 10000 workstation. The initial model of the GSH conjugate of (−)-*anti*-B[*c*]PDE was based on the crystal structure of mGSTA1-1 in complex with GSH conjugate of the activated diol epoxide of benzo[*a*]pyrene [(+)-*anti*-BPDE] (*31*), whereas the model for the GSH conjugate of (+)-*anti*-B[*c*]PDE was built by changing the absolute configuration of the corresponding carbon atoms. Both conjugates were subjected to geometry optimization using the conjugate gradient method of Powell (*32*) and docked into the active center of the mGSTA1-1·(+)-*anti*-BPDE−GSH conjugate complex (*31*) and that of the mGSTA2-2·(+)-*anti*-BPDE−GSH conjugate complex.[2] The BPDE moiety of the GSH conjugate of (+)-*anti*-BPDE assumes distinct binding modes in the two crystal structures[2] (*31*). Thus, the GSH conjugates of (−)- and (+)-*anti*-B[*c*]-PDE were docked into the active center of the two isoenzymes accordingly. All solvent molecules in the two crystal structures were excluded in the energy minimization of the mGSTA1-1·(−)-*anti*-B[*c*]PDE−GSH conjugate, the mGSTA1-1·(+)-*anti*-B[*c*]PDE−GSH conjugate, the mGSTA2-2·(−)-*anti*-B[*c*]PDE−GSH conjugate, and the mGSTA2-2·(+)-*anti*-B[*c*]PDE−GSH conjugate. The geometric parameters of Engh and Huber (*33*) were used as the basis of the force field.

RESULTS AND DISCUSSION

Enantioselectivity and Catalytic Activity of mGSTA1-1 and mGSTA2-2 toward anti-B[c]PDE Isomers. Figure 1 (panels A and B) depicts reverse-phase HPLC analysis of aqueous products resulting from the reaction of 2 mM GSH with racemic *anti*-B[*c*]PDE (320 μM) in the presence of mGSTA1-1 and mGSTA2-2 (15 μg/mL protein). As can be seen in Figure 1A, two peaks with retention times of ∼6.7 and ∼7.2 min, corresponding to GSH conjugates of (−)-*anti*- and (+)-*anti*-B[*c*]PDE, respectively, were observed in the reverse-phase HPLC chromatogram for mGSTA1-1. Fur-

[2] Y. Gu, S. V. Singh, and X. Ji, manuscript in preparation.

Table 3: Specific Activities of Wild-Type mGSTA1-1 and mGSTA2-2, and Their Chimeras, toward (−)- and (+)-*anti*-B[*c*]PDE

	specific activity (nmol min^{-1} mg^{-1})	
	(−)-*anti*-B[*c*]PDE	(+)-*anti*-B[*c*]PDE
wild-type enzyme		
mGSTA1-1	475 ± 60[a]	327 ± 33
mGSTA2-2	1867 ± 145[b]	41 ± 3[b]
chimeric enzyme		
section I of mGSTA1 and sections II and III of mGSTA2	1890 ± 91[b]	37 ± 2[b]
section II of mGSTA1 and sections I and III of mGSTA2	1459 ± 82[b,c]	68 ± 5[b,c]
section III of mGSTA1 and sections I and II of mGSTA2	522 ± 73[c]	242 ± 34[c]

[a] Data represent means ± standard deviation of at least three determinations. [b] Significantly different from that of wild-type mGSTA1-1 ($P < 0.05$). [c] Significantly different from that of wild-type mGSTA2-2 ($P < 0.05$).

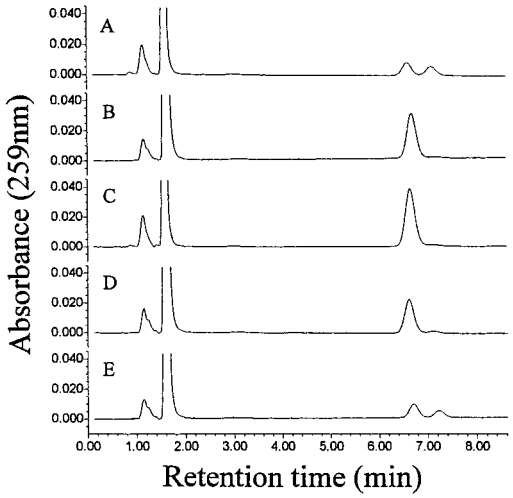

FIGURE 1: Reverse-phase HPLC chromatograms depicting GSH conjugation of (−)-*anti*- and (+)-*anti*-B[*c*]PDE upon incubation of 2 mM GSH with 320 μM (±)-*anti*-B[*c*]PDE in the presence of 15 μg/mL (A) wild-type mGSTA1-1, (B) wild-type mGSTA2-2, (C) chimeric enzyme containing section I of mGSTA1 and sections II and III of mGSTA2, (D) chimeric enzyme containing section II of mGSTA1 and sections I and III of mGSTA2, and (E) chimeric enzyme containing section III of mGSTA1 and sections I and II of mGSTA2. The details of the incubation and chromatographic conditions are described in Experimental Procedures.

thermore, even though mGSTA1-1 was found to catalyze the addition of GSH to both isomers of *anti*-B[*c*]PDE, it exhibited a slight preference for the (−)-*anti*-isomer since roughly 60% of the GSH conjugation occurred with this isomer (Figure 1A). The enantioselectivity was much more pronounced for mGSTA2-2 where >97% of the GSH conjugation occurred with the (−)-*anti*-B[*c*]PDE isomer (Figure 1B). The specific activities of mGSTA1-1 and mGSTA2-2 toward *anti*-B[*c*]PDE stereoisomers are summarized in Table 3. The specific activity of mGSTA2-2 toward (−)-*anti*-B[*c*]PDE, which is a much more potent tumor initiator than the (+)-*anti*-isomer in both the newborn mouse model and skin-tumorigenesis bioassay (*3*), was approximately 3.9-fold higher than that of mGSTA1-1. Taken together, these results indicate that mGSTA2-2 is significantly more active than mGSTA1-1 in the GSH conjugation of the (−)-*anti*-B[*c*]PDE isomer, and that the two isoenzymes differ markedly in their enantioselectivity toward *anti*-B[*c*]-PDE.

Specific Activities of the Chimeras of mGSTA1-1 and mGSTA2-2 toward anti-B[c]PDE. The differences in amino acid sequences between mGSTA1 and mGSTA2 are summarized in Table 1. These amino acid substitutions are distributed in three sections. Section I contains amino acid residues in positions 65 and 95; section II contains amino acid residues in positions 157, 162, and 169, and section III contains amino acid residues in positions 207, 213, 218, 221, and 222. To establish the contributions of these amino acid substitutions to catalytic differences between mGSTA1-1 and mGSTA2-2, section I, II, or III of mGSTA2-2 was replaced with the corresponding section of mGSTA1-1, followed by measurements of the activity of the chimeric enzymes toward *anti*-B[*c*]PDE. As can be seen in Table 3, the specific activity of the chimeric enzyme containing section I of mGSTA1-1 but sections II and III of mGSTA2-2 was comparable to that of wild-type mGSTA2-2. Likewise, replacement of section II of mGSTA2-2 with the equivalent portion of mGSTA1-1 did not have an appreciable effect on the specific activity toward (−)-*anti*-B[*c*]PDE (Table 3). The enantioselectivity of the chimeras involving section I or II was more or less similar to that of wild-type mGSTA2-2 (compare panels B−D of Figure 1). These results suggest that amino acid substitutions in section I or II may not be responsible for differences in enantioselectivity and catalytic activity between mGSTA1-1 and mGSTA2-2 toward *anti*-B[*c*]PDE. On the other hand, replacement of section III of mGSTA2-2 with the equivalent portion of mGSTA1-1 caused a statistically significant reduction in the activity of the protein. The specific activity of the chimeric enzyme containing section III of mGSTA1-1 and sections I and II of mGSTA2-2 was lower by ~72% compared with that of wild-type mGSTA2-2. Moreover, the enantioselectivity of this chimeric enzyme became comparable to that of wild-type mGSTA1-1 (compare panels A and E of Figure 1). Taken together, these observations clearly indicate that amino acid substitutions in section III are responsible for catalytic differences between mGSTA1-1 and mGSTA2-2 with respect to *anti*-B[*c*]PDE.

Activities of Site-Directed Mutants of mGSTA2-2. To identify the residue(s) in section III responsible for catalytic differences between the two proteins, amino acid residues in positions 207, 213, 218, 221, and 222 of mGSTA2-2 were replaced with the equivalent portion of mGSTA1-1 by PCR-based site-directed mutagenesis. Subsequently, the mutant enzymes together with wild-type mGSTA1-1 and mGSTA2-2 were examined for their activity toward *anti*-B[*c*]PDE, and the results are shown in Table 4. Unlike that of wild-type mGSTA1-1 (Figure 1), the GSH conjugation of (+)-*anti*-B[*c*]PDE isomer was not evident in the presence of any of the mutants, suggesting that all five residues may be required for the expression of activity toward the (+)-*anti*-isomer of B[*c*]PDE. Specific activities toward (−)-*anti*-B[*c*]PDE of the mutants involving residues in positions 213 and 222 were

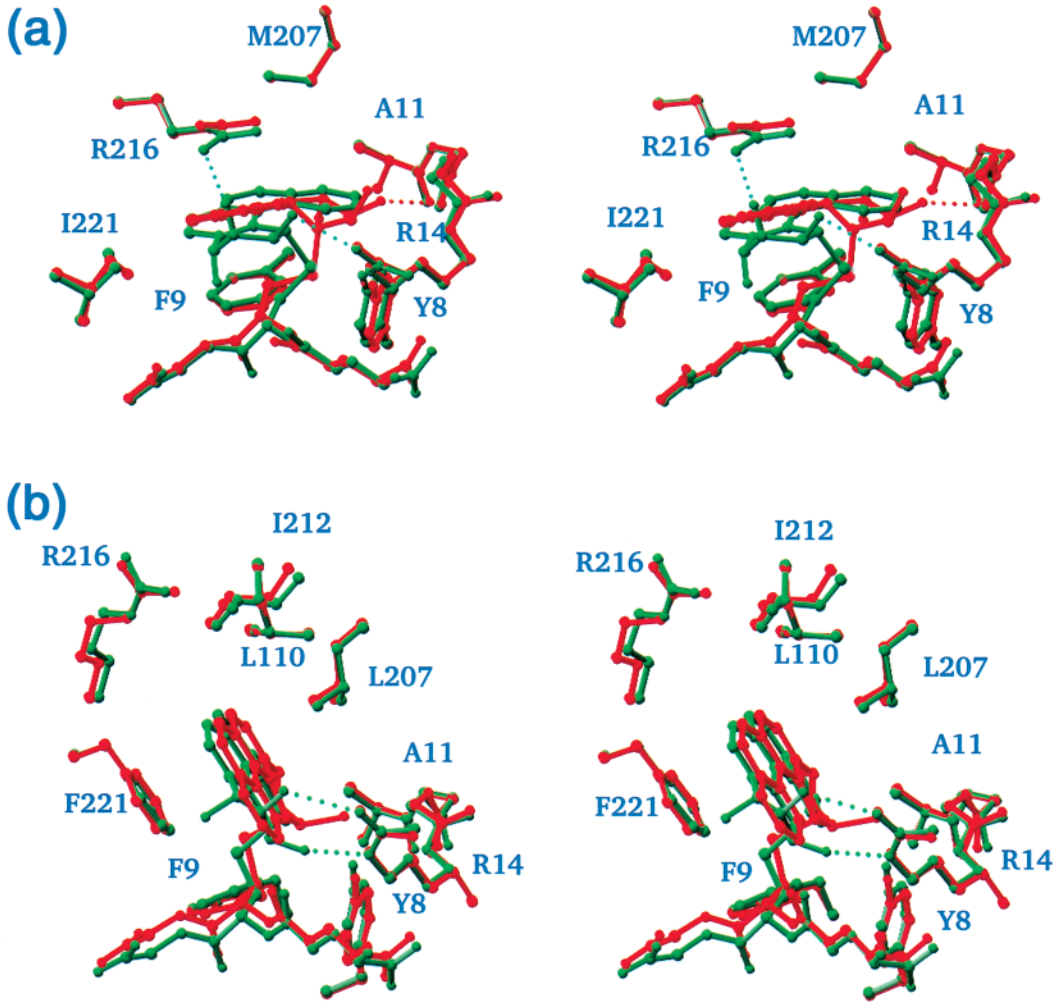

FIGURE 2: Stereo representations showing the active center in the models of (a) the mGSTA1-1·(−)-*anti*-B[*c*]PDE−GSH conjugate (green) and the mGSTA1-1·(+)-*anti*-B[*c*]PDE−GSH conjugate (red) and (b) the mGSTA2-2·(−)-*anti*-B[*c*]PDE−GSH conjugate (green) and the mGSTA2-2·(+)-*anti*-B[*c*]PDE−GSH conjugate (red). Protein residues and product molecules are represented by ball-and-stick models. Hydrogen bonds are depicted as dashed lines. The figure was prepared using RIBBONS (*35*).

Table 4: Specific Activities of Wild-Type mGSTA2-2 and Its Mutants toward (−)-*anti*-B[*c*]PDE[a]

enzyme	specific activity (nmol min^{-1} mg^{-1})
wild-type mGSTA2-2	1491 ± 73[b]
wild-type mGSTA1-1	414 ± 48[c]
L207M mutant of mGSTA2-2	445 ± 57[c]
E213Q mutant of mGSTA2-2	1182 ± 37[c]
V218A mutant of mGSTA2-2	1482 ± 356
F221I mutant of mGSTA2-2	841 ± 50[c]
−222Q mutant of mGSTA2-2	1153 ± 295

[a] Unlike wild-type mGSTA1-1, a peak corresponding to GSH conjugate of (+)-*anti*-B[*c*]PDE was not detectable in the presence of any of the mutants, suggesting that all five residues in section III may be necessary for the expression of activity toward the (+)-*anti*-isomer of B[*c*]PDE. [b] Values are means ± standard deviations of three determinations. [c] Significantly different from that of wild-type mGSTA2-2 ($P < 0.05$).

slightly lower (~21−23%) in comparison with that of wild-type mGSTA2-2, suggesting that these residues may play a limited role, if any, in the activity differences between mGSTA1-1 and mGSTA2-2. Likewise, the amino acid residue in position 218 may not account for catalytic differences between the two isoenzymes since the activity of the V218A mutant of mGSTA2-2 was more or less similar to that of wild-type mGSTA2-2 (Table 4). On the other hand, replacement of amino acid residues in position 207 or 221 resulted in a statistically significant reduction in the activity toward (−)-*anti*-B[*c*]PDE. The specific activities of the L207M and F221I mutants toward (−)-*anti*-B[*c*]PDE were lower by ~70 and ~44%, respectively, than that of wild-type mGSTA2-2 (Table 4). Interestingly, the specific activity of the L207M mutant was more or less similar to that of wild-type mGSTA1-1. These results suggest that L207 and F221 may contribute to catalytic differences between mGSTA1-1 and mGSTA2-2 with respect to (−)-*anti*-B[*c*]PDE.

Molecular Modeling Studies. Modeling studies were carried out to understand the molecular basis for catalytic differences between mGSTA1-1 and mGSTA2-2 toward *anti*-B[*c*]PDE, and the results are shown in Figure 2. The differential enantioselectivity of the two isoenzymes toward *anti*-B[*c*]PDE isomers can be explained on the basis of differences in the interactions between their active site residues and the hydroxyl groups at positions 2 and 3 of the product molecule (Figure 2). A comparison of the model structures of mGSTA1-1 in complex with the GSH conjugate of (−)-*anti*-B[*c*]PDE (Figure 2a, shown in green) and mGSTA1-1 in complex with the GSH conjugate of (+)-*anti*-B[*c*]PDE (Figure 2a, shown in red) reveals two major

differences. First, the guanidino group of R216 maintains a hydrogen bond with the hydroxyl group at position 3 of the GSH conjugate of (−)-*anti*-B[*c*]PDE (Figure 2a, green), which makes possible the assistance of R216 in the epoxide ring-opening reaction (*31*). This interaction was not apparent in the model of the mGSTA1-1•(+)-*anti*-B[*c*]PDE−GSH conjugate (Figure 2a, red). Second, the guanidino group of R14 forms a hydrogen bond with the hydroxyl group at position 2 of the GSH conjugate of (−)-*anti*-B[*c*]PDE, suggesting that the previously demonstrated catalytic role of R14 (*34*) is not interrupted. This interaction was also absent in the model of the mGSTA1-1•(+)-*anti*-B[*c*]PDE−GSH conjugate (Figure 2a, red). In addition, there is an unfavorable short contact between the hydroxyl group at position 3 and G13 in the model of the mGSTA1-1•(+)-*anti*-B[*c*]PDE−GSH conjugate. These results suggest that mGSTA1-1 may have a slight preference for (−)-*anti*-B[c]-PDE over the (+)-*anti*-isomer, which was experimentally verified during enzyme activity determinations (Table 3).

A comparison of the model structures of the mGSTA2-2•(−)-*anti*-B[*c*]PDE−GSH conjugate (Figure 2b, green) and the mGSTA2-2•(+)-*anti*-B[*c*]PDE−GSH conjugate (Figure 2b, red) suggests that the (−)-*anti*-isomer may be a better substrate than (+)-*anti*-B[*c*]PDE for mGSTA2-2, which was experimentally verified during activity measurements (Table 3). Both hydroxyl groups 2 and 3 of the GSH conjugate of (−)-*anti*-B[*c*]PDE form hydrogen bonds with the guanidino group of R14, whereas these interactions are not possible for the (+)-*anti*-B[*c*]PDE−GSH conjugate. The lack of favorable interactions between the (+)-*anti*-B[*c*]PDE−GSH conjugate and mGSTA2-2 is exacerbated by the presence of unfavorable short contacts between hydroxyl groups at positions 2 and 3 of the (+)-*anti*-B[*c*]PDE−GSH conjugate and active site residues G13 and F9, respectively, of mGSTA2-2. Consequently, mGSTA2-2 is extremely poor in catalyzing the addition of GSH to (+)-*anti*-B[*c*]PDE (Table 3). Although with the results of molecular modeling studies we are able to interpret the distinct enantioselectivity of mGSTA1-1 and mGSTA2-2, they are not sufficient to interpret the differences in their catalytic activity toward (−)-*anti*-B[*c*]PDE. Elucidation of the molecular mechanism for the activity difference between mGSTA1-1 and mGSTA2-2 with respect to (−)-*anti*-B[*c*]PDE would require crystal structure determinations of these isoenzymes in complex with a transition state analogue.

CONCLUSIONS

The results of the study presented here reveal that mGSTA2-2 is relatively more active than mGSTA1-1 in catalyzing the GSH conjugation of the (−)-*anti*-B[*c*]PDE isomer, suggesting that mGSTA2-2 may play an important role in the detoxification of B[*c*]PDE. The overall contribution of mGSTA2-2 to defense against the carcinogenic effects of B[*c*]PDE is likely to be even higher due to its preference for the (−)-*anti*-isomer. Our results also indicate that amino acid substitutions in the C-terminal region, particularly amino acid residues in positions 207 and 221, are responsible for differential enantioselectivity of mGSTA1-1 and mGSTA2-2 with respect to *anti*-B[*c*]PDE.

ACKNOWLEDGMENT

We thank Hong Xia for assistance in preparation of chimeric and mutant enzymes.

REFERENCES

1. International Agency for Research on Cancer (1983) *IARC Monographs on the Evaluation of the Carcinogenic Risk of Chemicals to Humans. Polynuclear Aromatic Compounds. Part 1. Chemical, Environmental, and Experimental Data*, Vol. 32, International Agency for Research on Cancer, Lyon, France.
2. Sims, P., and Grover, P. L. (1974) *Adv. Cancer Res. 20*, 165−274.
3. Levin, W., Chang, R. L., Wood, A. W., Thakker, D. R., Yagi, H., Jerina, D. M., and Conney, A. H. (1986) *Cancer Res. 46*, 2257−2261.
4. Oesch, F., Schladt, L., Knehr, M., Doehmer, J., and Thomas, H. (1991) in *NATO ASI Live Sciences Series. Molecular Aspects of Monooxygenases and Bioactivation of Toxic Compounds* (Arinc, E., Schenkman, J. B., and Hodgson, E., Eds.) pp 435−445, Plenum Press, New York.
5. Thakker, D. R., Yagi, H., Levin, W., Wood, A. W., Conney, A. H., and Jerina, D. M. (1985) in *Polycyclic Aromatic Hydrocarbons: Metabolic Activation to Ultimate Carcinogens. Bioactivation of Foreign Compounds* (Anders, M. W., Ed.) pp 177−242, Academic Press, New York.
6. Dipple, A. (1985) in *Polycyclic Hydrocarbons and Carcinogenesis. Polycyclic Aromatic Hydrocarbon Carcinogenesis: An Introduction.* (Harvey, R. G., Ed.) ACS Symposium Series 283, pp 1−17, American Chemical Society, Washington, DC.
7. Yang, S. K., and Gelboin, H. V. (1976) *Cancer Res. 36*, 4185−4189.
8. Dock, L., Waern, F., Martinez, M., Grover, P. L., and Jernström, B. (1986) *Chem.-Biol. Interact. 58*, 301−318.
9. Lu, A. Y. H., Jerina, D. M., and Levin, W. (1977) *J. Biol. Chem. 252*, 3715−3723.
10. Robertson, I. G. C., Guthenberg, C., Mannervik, B., and Jernström, B. (1986) *Cancer Res. 46*, 2220−2224.
11. Funk, M., Gath, I., Seidel, A., Platt, K. L., Oesch, F., and Zeller, H. D. (1994) *Biochem. Pharmacol. 47*, 505−514.
12. Funk, M., Gath, I., Seidel, A., Oesch, F., and Platt, K. L. (1995) *Chem.-Biol. Interact. 95*, 189−201.
13. Hu, X., Srivastava, S. K., Xia, H., Awasthi, Y. C., and Singh, S. V. (1996) *J. Biol. Chem. 271*, 32684−32688.
14. Hu, X., Herzog, C., Zimniak, P., and Singh, S. V. (1999) *Cancer Res. 59*, 2358−2362.
15. Mannervik, B. (1985) *Adv. Enzymol. Relat. Areas Mol. Biol. 57*, 357−417.
16. Hayes, J. D., and Pulford, D. J. (1995) *Crit. Rev. Biochem. Mol. Biol. 30*, 445−600.
17. Mannervik, B., Alin, P., Guthenberg, C., Jensson, H., Tahir, M. K., Warholm, M., and Jornvall, H. (1985) *Proc. Natl. Acad. Sci. U.S.A. 82*, 7202−7206.
18. Meyer, D. J., Coles, B., Pemble, S. E., Gilmore, K. S., Fraser, G. M., and Ketterer, B. (1991) *Biochem. J. 274*, 409−414.
19. Board, P. G., Baker, R. T., Chelvanayagam, G., and Jermiin, L. S. (1997) *Biochem. J. 328*, 929−935.
20. Hu, X., Seidel, A., Frank, H., Srivastava, S. K., Xia, H., Pal, A., Zheng, S., Oesch, F., and Singh, S. V. (1998) *Arch. Biochem. Biophys. 358*, 40−48.
21. Hu, X., Benson, P. J., Srivastava, S. K., Mack, L. M., Xia, H., Gupta, V., Zaren, H. A., and Singh, S. V. (1996) *Arch. Biochem. Biophys. 336*, 199−214.
22. Hu, X., and Singh, S. V. (1997) *Arch. Biochem. Biophys. 340*, 279−286.
23. Xia, H., Pan, S.-S., Hu, X., Srivastava, S. K., Pal, A., and Singh, S. V. (1998) *Arch. Biochem. Biophys. 353*, 337−348.
24. Habig, W. H., Pabst, M. J., and Jakoby, W. B. (1974) *J. Biol. Chem. 249*, 7130−7139.
25. Bradford, M. M. (1976) *Anal. Biochem. 72*, 248−254.
26. Xia, H., Gu, Y., Pan, S.-S., Ji, X., and Singh, S. V. (1999) *Biochemistry 38*, 9824−9830.

27. Simons, P. C., and Vander Jagt, D. L. (1977) *Anal. Biochem. 82*, 334−341.
28. Laemmli, U. K. (1970) *Nature 227*, 680−685.
29. Brunger, A. T., and Rice, L. M. (1997) *Methods Enzymol. 277*, 243−269.
30. Jones, T. A., and Kjeldgaard, M. (1997) *Methods Enzymol. 277*, 173−208.
31. Gu, Y., Singh, S. V., and Ji, X. (2000) *Biochemistry 39*, 12552−12557.
32. Powell, M. J. D. (1977) *Math. Prog. 12*, 241−254.
33. Engh, R. A., and Huber, R. (1991) *Acta Crystallogr. A47*, 392−400.
34. Nanduri, B., Hayden, J. B., Awasthi, Y. C., and Zimniak, P. (1996) *Arch. Biochem. Biophys. 335*, 305−310.
35. Carson, M. (1987) *J. Mol. Graphics 5*, 103−106.

BI010363R